Recent Improvements to the IMPACT-T Parallel Particle Tracking Code *

J. Qiang†, I. V. Pogorelov, R. Ryne, LBNL, Berkeley, CA 94547, USA

Abstract

The IMPACT-T code is a parallel three-dimensional quasi-static beam dynamics code for modeling high brightness beams in photoinjectors and RF linacs. Developed under the US DOE Scientific Discovery through Advanced Computing (SciDAC) program, it includes several key features including a self-consistent calculation of 3D space-charge forces using a shifted and integrated Green function method, multiple energy bins for beams with large energy spread, and models for treating RF standing wave and traveling wave structures. In this paper, we report on recent improvements to the IMPACT-T code including modeling traveling wave structures, short-range transverse and longitudinal wakefields, and longitudinal coherent synchrotron radiation through bending magnets.

INTRODUCTION

IMPACT-T is a fully three-dimensional parallel program to track relativistic particles taking into account space charge forces, short-range longitudinal and transverse wakefields, and coherent synchrotron radiation (CSR). It has a comprehensive set of beamline elements, and furthermore allows arbitrary overlap of their fields, which gives the IMPACT-T code a capability to model both standing wave and traveling wave structures. It is also unique in its use of space-charge solvers based on an integrated Green function to efficiently and accurately treat beams with large aspect ratio, and a shifted Green function to efficiently treat image charge effects of a cathode [1]. It is also unique in its inclusion of energy binning in the space-charge calculation to model beams with large energy spread. IMPACT-T has a flexible data structure that allows particles to be stored in containers with common characteristics; for photoinjector simulations the containers represent multiple slices, but in other applications they could correspond, e.g., to particles of different species. The IMPACT-T code has been used to study the beam dynamics at a number of photoinjectors such as the Fermilab A0 photoinjector, LCLS normal RF injector, Cornell ERL DC injector, BNL superconducting photoinjector, and others.

* Work supported by a Scientific Discovery through Advanced Computing project, "Advanced Computing for 21st Century Accelerator Science and Technology," which is supported by the US DOE/SC Office of High Energy Physics and the Office of Advanced Scientific Computing Research.

† jqiang@lbl.gov

PHYSICAL MODELS

The general equations of motion used in the IMPACT-T code are:

$$\dot{\mathbf{r}} = \frac{\mathbf{p}}{m\gamma} \quad (1)$$

$$\dot{\mathbf{p}} = q(\mathbf{E} + \frac{\mathbf{p}}{m\gamma} \times \mathbf{B}) \quad (2)$$

where, $\gamma = 1/\sqrt{1-\beta^2}$, $\beta_i = v_i/c$ with $i = x, y, z$, c is the speed of light, m is the rest mass of a particle, q is the charge of a particle. The electric field, $\mathbf{E}$, and magnetic field, $\mathbf{B}$, include the contributions from external focusing and accelerating fields and space-charge fields of intra-particle Coulomb interactions. For an RF linac, under proper gauge ($\phi = 0$), the external electromagnetic fields in a cylindrically symmetric accelerating structure can be obtained from [2]:

$$\mathbf{E} = -\frac{\partial \mathbf{A}}{\partial t} \quad (3)$$

$$\mathbf{B} = \nabla \times \mathbf{A} \quad (4)$$

where the vector potential $\mathbf{A}$ is given by

$$A_x = \frac{1}{\omega} x \sum_{n=0}^{\infty} \frac{1}{2(n+1)} e_n'(z) r^{2n} \sin(\omega t + \theta) \quad (5)$$

$$A_y = \frac{1}{\omega} y \sum_{n=0}^{\infty} \frac{1}{2(n+1)} e_n'(z) r^{2n} \sin(\omega t + \theta) \quad (6)$$

$$A_z = -\frac{1}{\omega} \sum_{n=0}^{\infty} e_n'(z) r^{2n} \sin(\omega t + \theta) \quad (7)$$

with $r^2 = x^2 + y^2$ and

$$e_{n+1}(z) = -\frac{1}{4(n+1)^2} (e_n''(z) + \frac{\omega^2}{c^2} e_n(z)) \quad (8)$$

where $e_0(z)$ is the electric field on the axis, ω is the RF angular frequency, θ is the initial phase of the RF field with respect to global time zero, and a superscript prime denotes the derivative with respect to z. In the current version of the code, n is up to 1 in the above equations summation so that only second order and third order nonlinearity are included for off-axis fields. If the RF cavity does not have cylindrical symmetry, the fully three-dimensional electromagnetic fields are read in from external data files. The electromagnetic fields in a traveling wave structure can be viewed as having the form of a standing wave around the entrance and the exit of the structure, and a traveling wave in most cells

between. In IMPACT-T traveling wave structures are modeled using a superposition of two standing waves. Here, the traveling wave field on the axis is given by [3]:

$$E_t(z,t) = \frac{1}{\sin(\beta_0 d)}(E_s(z)\cos(\omega t + \beta_0 d - \pi/2 + \theta) + E_s(z+d)\cos(\omega t + \pi/2 + \theta)) \quad (9)$$

where, $E_s(z)$ is the electric field of a standing wave, d is the length of a single cell, $\beta_0 = \omega/c$, and θ is the initial driven phase of the wave, which is the same as that in the entrance and exit standing wave fields. To check the correctness of the above implementation, we run a particle on axis through a $2\pi/3$ traveling wave structure at LCLS. The longitudinal electric field observed by the particle as a function of distance is shown in Fig. 1 for the first 1.5 meter. We see that the field varies smoothly from the entrance

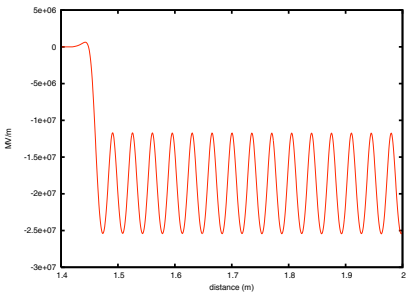

Figure 1: Longitudinal electric field as a function of distance through a traveling wave structure.

standing wave cell into the traveling wave cells. The same is also true for the field through the exit cell.

The space-charge forces are calculated by solving the 3D Poisson equation with open boundary conditions using an integrated Green function method. The image charge effects of the conducting cathode are also included using a shifted Green function method. A detailed description of the space-charge solver can be found in reference [1]. Besides the space-charge forces, the short range longitudinal wake field (monopole) and transverse wake field (dipole) are also included. The effective forces from the wake fields are given as:

$$F_x(s) = q\int_s^{\infty} W_T(s-s')x(s')\lambda(s')ds' \quad (10)$$

$$F_z(s) = q\int_s^{\infty} W_L(s-s')\lambda(s')ds' \quad (11)$$

where W_T is the transverse wake function, W_L is the longitudinal wake field function, and λ is the line density function of the beam. To compute the effective forces from wake fields more efficiently, we extend the above integrals into a full domain convolution as:

$$F(s) = \int_{-\infty}^{+\infty} G(s-s')\rho(s')ds' \quad (12)$$

where

$$G(s) = \begin{cases} W(s) & for\ s \le 0 \\ 0 & for\ s > 0 \end{cases} \quad (13)$$

$$\rho(s) = \begin{cases} x(s)\lambda(s) & for\ transverse\ wake \\ \lambda(s) & for\ longitudinal\ wake \end{cases} \quad (14)$$

The above convolution is calculated using an FFT-based method on a doubled computational domain. Fig. 2 shows a comparison of computational operations required to calculate the effective wake forces from using direct summation and from using the FFT-based method. It is seen that after

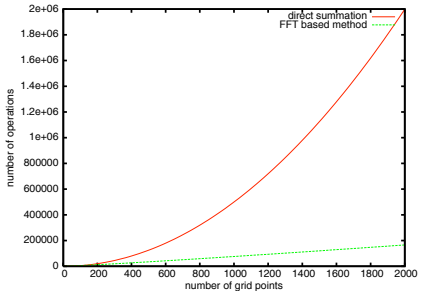

Figure 2: Computational operations required for the effective wake force calculation as a function of grid number by using direct summation and by using the FFT method.

around 200 grid points, the FFT-based method is more efficient than the direct summation. Here, the doubled computational grid is included in the calcuation of computational operations of the FFT-based method.

The bending magnet in the IMPACT-T code is modeled as a constant vertical field region and two fringe field regions on both ends of the magnet. At the entrance of the bending magnet, a Cartesian coordinate is set. A schematic plot of the layout of a bending magnet in this local coordinate system is shown in Fig. 3. The pole faces of the

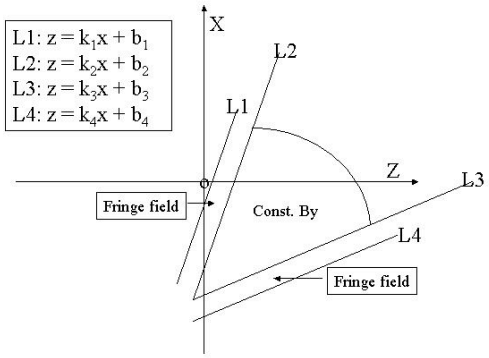

Figure 3: A schematic plot of the layout of a bending magnet in a local Cartesian coordinate system.

bending magnet at the entrance and the exit are described

by four linear equations:

$$z = k_i x + b_i \quad (15)$$

where i is from 1 to 4 corresponding to the four edge lines defining the fringe field and the center field regions in the figure. A reference particle is defined with only initial longitudinal components from the centroid of the beam in the local coordinate system. Inside the bend, both simulated macroparticles and the reference particle are advanced using the dipole magnetic fields. To calculate the space-charge forces or CSR forces, we transform the macroparticle coordinates into a coordinate system originating at the reference particle through rotation. A momentum kick is done inside the reference particle coordinate system and transformed back to the local coordinate system. When the beam is out of the bending magnet, all macroparticles are rotated again into the reference particle coordinate system. This gives the macroparticle local coordinates in the next beam line element. Here, we have assumed that the reference particle will move through the axis of the bending magnet and into the axis of the next element. Fig. 4 shows a comparison of a phase space distribution after a bending magnet chicane from the above model and from the MARYLIE model. The two models agree well in this case.

CSR is modeled as a one-dimensional (1D) longitudinal wake field. The model implemented in the current version of IMPACT-T is a 1D, steady-state model (long magnet, no transient effects) as described in Ref. [4], where the change of energy due to CSR is given by:

$$\frac{dE}{cdt} = -\frac{2e^2}{4\pi\epsilon_0 3^{1/3} R^{2/3}} \int_{-\infty}^{s} \frac{1}{(s-s')^{1/3}} \frac{d\lambda(s')}{ds'} ds' \quad (16)$$

Numerical evaluation of this expression is complicated by the fact that the integral operator kernel is weakly singular, and the linear charge density that it operates on is contaminated by numerical noise. As described in Ref. [5] , our approach is based on a combination of integration-by-parts, use of custom-designed filters, and treating differently–for the purpose of numerical integration–the regions near and away from the singularity of the integral term's kernel. Fig. 5 shows the results of testing the new CSR routine by simulation of the passage through a single bend magnet of a distribution composed of 2 million particles all having equal energy, but with a sinusoidal charge density modulation in the z-direction. The solid blue line is the theoretical prediction, seen to be in a very good agreement with the numerical simulation result, shown in red. It was confirmed in separate tests that the local energy spread in the final distribution is due to non-zero transverse emittance of the initial distribution. What appears to be a solid horizontal line at $\Delta\gamma = 0$ is an initial distribution footprint in the longitudinal phase space.

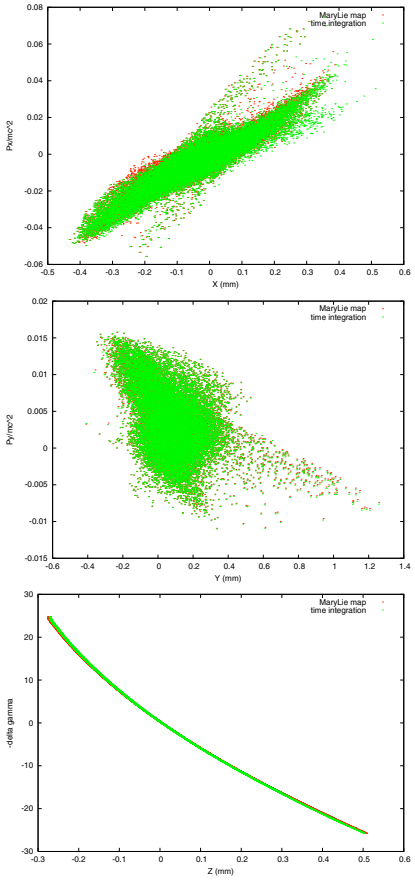

Figure 4: Transverse and longitudinal phase space distribution after a bending magnet chicane from the time integration model of IMPACT-T and from the MARYLIE map model.

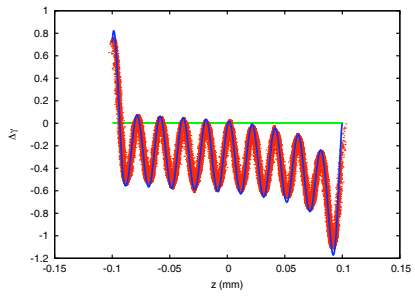

Figure 5: Longitudinal phase space distribution after a bending magnet for an initial sinusoid density modulation.

REFERENCES

[1] J. Qiang, S. Lidia, R. D. Ryne, C. Limborg-Deprey, Phys. Rev. Special Topics - Accel. Beams, 9 (2006) 044204.

[2] P. L. Morton, Particle Dynamics in Linear Accelerators, Ph. D. Thesis, Midwestern Universities Research Association, The Ohio State University, 1963.

[3] G. A. Loew, R. H. Miller, R. A. Early and K. L. Bane, SLAC-PUB-2295 (1979).

[4] E.L. Saldin, E.A. Schneidmiller, and M.V. Yurkov, Nucl. Instrum. Methods Phys. Res., Sect. A 398, 373 (1997).

[5] I. Pogorelov et al., "Recent Developments in IMPACT and Application to Future Light Sources," this proceedings.